Electrochemistry Communications 169 (2024) 107823

Contents lists available at ScienceDirect

Electrochemistry Communications

journal homepage: www.elsevier.com/locate/elecom

The influence of acetone and isopropanol crossover on the direct isopropanol fuel cell

Dominik Venus [a,b], Moritz Valeske [a,b], Matthew Brodt [b], Peter Wasserscheid [b,c,d], Simon Thiele [a,b,*]

[a] Forschungszentrum Jülich GmbH, Helmholtz-Institute Erlangen-Nürnberg for Renewable Energy (IET-2), Electrocatalytic Interface Engineering, Cauerstrasse 1, 91054 Erlangen, Germany
[b] Department of Chemical and Biological Engineering, Friedrich-Alexander-University (FAU), Erlangen and Nürnberg, Erlangen, Germany
[c] Forschungszentrum Jülich GmbH, Helmholtz-Institute Erlangen-Nürnberg (IET-2), Chemical Hydrogen Storage, Cauerstrasse 1, 91054 Erlangen, Germany
[d] Forschungszentrum Jülich GmbH, Institute for a Sustainable Hydrogen Economy, Am Brainergy Park 4, 52428 Jülich, Germany

ARTICLE INFO

Keywords:
Direct alcohol fuel cell (DAFC)
Direct isopropanol fuel cell (DIFC)
Electro-oxidation of alcohols
Liquid organic hydrogen carriers (LOHC)
Electrochemical addressable LOHC (EC-LOHC)

ABSTRACT

Liquid organic hydrogen carriers (LOHC) offer a promising option to store and release hydrogen on demand within existing infrastructure. The direct isopropanol fuel cell (DIFC) uses the electrochemical acetone/isopropanol LOHC couple and combines the advantages of high fuel energy density at ambient conditions with CO_2-free direct electricity production. Like other alcohol fuel cells, the DIFC combines two kinetically slow reactions, the isopropanol oxidation reaction (IOR) and the oxygen reduction reaction (ORR), requiring considerable overpotentials to drive the reactions. Accordingly, deconvoluting kinetic characteristics in the full cell is difficult. Therefore, this work uses the electrolytic electrochemical dehydrogenation unit (EDU), consisting of the IOR and the kinetically fast hydrogen evolution reaction in acidic media. This EDU then serves as an IOR full-cell model to get insights on the DIFC. Correspondingly, the demonstrated work is a comparison study investigating in-house fabricated catalyst-coated membrane electrode assemblies as hydrogen fuel cells, DIFC, and EDU. It investigates characteristic features of the DIFC and demonstrates how the acetone and isopropanol crossover affect the cathode of the DIFC.

1. Introduction

Direct alcohol fuel cells (DAFCs) are a promising fuel cell type that combines high fuel energy density at ambient conditions and easy liquid handling within existing infrastructure [1]. The best-known direct alcohol fuel cell is the direct methanol fuel cell (DMFC), which oxidizes methanol to water and CO_2 while generating electricity [2]. However, considering the necessity of a CO_2-free energy infrastructure, DMFCs have an intrinsic drawback. A possible alternative to DMFCs is the direct isopropanol (2-propanol, IPA) fuel cell (DIFC, Fig. 1) that combines the advantages of high fuel energy density at ambient conditions with CO_2-free electricity production [3]. The two half-cell reactions of the DIFC are the anodic isopropanol oxidation reaction (IOR) and the cathodic oxygen reduction reaction (ORR), resulting in a galvanic cell converting chemical energy directly to electricity.

In contrast to primary alcohols, secondary alcohols like isopropanol can be oxidized selectively without breaking any C—C bond, forming the corresponding ketone acetone (ACE), protons, and electrons [4,5]. Acetone, in turn, can be either thermocatalytically or electrochemically reduced to isopropanol, closing a CO_2 emission-free hydrogen storage cycle [6–8]. Accordingly, the ACE/IPA couple is a liquid organic hydrogen carrier (LOHC), whereby acetone corresponds to the hydrogen-lean LOHC− and isopropanol to the hydrogen-rich LOHC+ [9]. While most LOHC systems thermocatalytically store and release hydrogen on demand, the ACE/IPA couple is a low-temperature electrochemical LOHC system. To differentiate these low-temperature electrochemical LOHCs from thermocatalytical LOHCs, the term electrochemical liquid organic hydrogen carrier (EC-LOHC) has been introduced [10].

The DIFC membrane-electrode-assembly (MEA) polarization curves with PtRu as the IOR catalyst expose two unique characteristics distinguishing them from other direct alcohol fuel cells (Fig. 2):

* Corresponding author at: Forschungszentrum Jülich GmbH, Helmholtz-Institute Erlangen-Nürnberg for Renewable Energy (IET-2), Electrocatalytic Interface Engineering, Cauerstrasse 1, 91054 Erlangen, Germany.
E-mail address: si.thiele@fz-juelich.de (S. Thiele).

https://doi.org/10.1016/j.elecom.2024.107823
Received 5 September 2024; Received in revised form 30 September 2024; Accepted 9 October 2024
Available online 21 October 2024
1388-2481/© 2024 The Authors. Published by Elsevier B.V. This is an open access article under the CC BY license (http://creativecommons.org/licenses/by/4.0/).

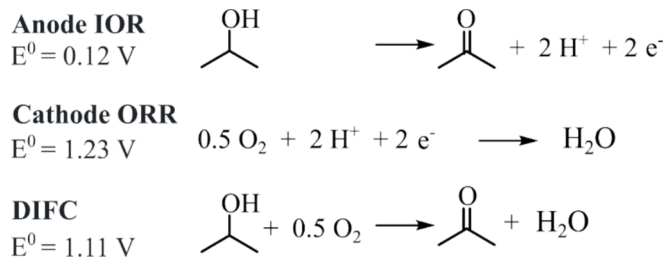

Fig. 1. Reaction equations in acidic environments and standard reaction potentials (E^0) for the DIFC.

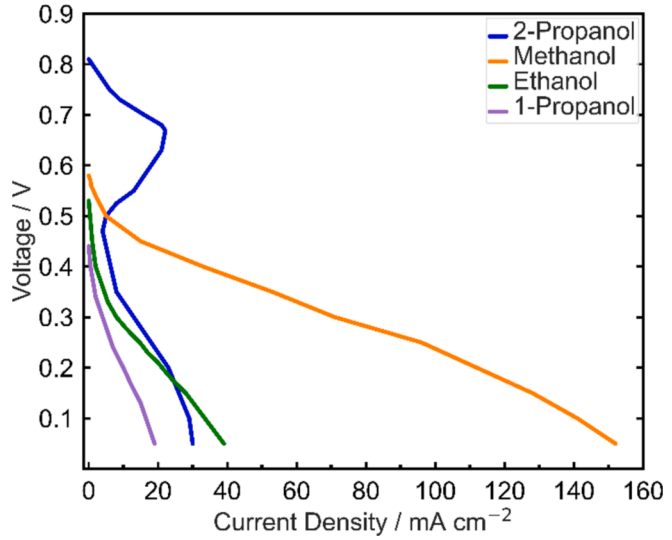

Fig. 2. DAFC MEA polarization curves for aqueous 1 M alcohol solutions at 50 °C with a dry oxygen cathode feed. Anode 2 mg_{PtRu} cm^{-2}, N115 membrane, Cathode 2 $mg_{Pt}cm^{-2}$. Reproduced with permission [13]. Copyright 2009, Johnson Matthey.

(a) The DIFC open circuit voltage (OCV) is at about 800 –750 mV in contrast to 650–550 mV for comparable DMFCs or 550–500 mV for comparable direct ethanol fuel cells (DEFC) when using PFSA membranes [3,11–14].
(b) A double-peak phenomenon exists in the polarization curve, with the first peak appearing at about 0.65 V [3,9,15].

The OCV is a reflection of the reversible cell potential (E_{rev}) impaired by the effect of the internal currents caused by fuel crossover or catalyst surface oxides [16,17]. In fact, the high experimental DIFC OCV is not based on thermodynamics as E_{rev} is the lowest for the DIFC (of the DAFCs within Fig. 2), whereas the highest for the DMFC [18–21]. Accordingly, the high DIFC OCV is either due to a lower ACE/IPA fuel crossover or smaller effects of the internal currents caused by the fuel crossover on the OCV [11].

Khanipour et al. [5] explained the two separated IOR peaks with different active catalyst sites. In a three-electrode scanning flow cell setup, they showed that Pt exhibits only one IOR peak at 0.75 V vs. the reversible hydrogen electrode (RHE). Bimetallic PtRu, however, reveals an additional early IOR peak at 0.18 V vs. RHE. They also confirmed via electrochemical real-time mass spectrometry that the early IOR at PtRu forms no CO_2 [4,5,22]. This early IOR oxidation peak at 0.18 V vs. RHE can probably be attributed to the early IOR peak in a DIFC with a PtRu anode catalyst. *Hauenstein et al.* [23] demonstrated that the early DIFC peak shifts with the PtRu loading: The higher the PtRu loading, the higher the reaction rate, and the lower the voltage at which the characteristic voltage drop sets in. Hence, the higher the PtRu loading, the lower the required anode potential for a given reaction rate.

In general, MEA tests best represent state-of-the-art electrocatalytic technology close to an application. However, like other DAFCs, the DIFC represents a combination of two kinetically slow reactions, the IOR and the ORR, requiring considerable overpotentials to drive the reactions. Accordingly, deconvoluting particular kinetic characteristics of the individual electrode reactions is difficult.

Therefore, this work uses a MEA concept that combines the anodic IOR with the cathodic hydrogen evolution reaction (HER) and compares it to the DIFC. This electrochemical dehydrogenation unit (EDU) consists of the anodic IOR and the cathodic HER in acidic media using a proton exchange membrane (PEM), producing hydrogen upon polarization (Fig. 3a). The HER at Pt in acidic environments is among the fastest known electrochemical reactions with negligibly small overpotentials to drive the reaction [24,25]. Thus, the EDU can serve as a model system to get full-cell information on the IOR without the influence of the kinetically slow ORR.

In the literature, the electrochemical dehydrogenation is also known as electrochemical reforming or electro-oxidation of alcohols [26,27]. The electrochemical dehydrogenation of methanol and ethanol has drawn significant attention in recent years [28–40]. However, like the DMFC, those dehydrogenation units form CO_2 as a dehydrogenation product.

The following work is a comparison study investigating in-house fabricated catalyst-coated membrane (CCM) MEAs as hydrogen fuel cells (H_2PEMFC), DIFC, and EDU, providing kinetic information regarding the IOR and ORR for the DIFC and information regarding the influence of an acetone and isopropanol fuel crossover (Fig. 3). Moreover, rotating disk electrode (RDE) experiments investigate the impact of acetone and isopropanol on the ORR, mimicking the acetone/isopropanol fuel crossover in the DIFC.

2. Theory and cacluclations

2.1. Thermodynamics of the DIFC and EDU

The IOR is an endothermic reaction that needs heat and electric work of at least 44.87 kJ mol^{-1} and 0.118 V at standard conditions (E^0) [18,19]. Combining the IOR with the exergonic ORR results in the DIFC, a galvanic cell that can provide electric work and heat upon polarization. Accordingly, the DIFC should generate a voltage as high as possible at a given reaction rate.

The EDU combines the IOR and the HER (Fig. 3), resulting in an electrolytic or electrolysis cell producing hydrogen and acetone upon polarization. Accordingly, the EDU cell should maintain a voltage as low as possible at a given reaction rate.

$E_{rev}(=E_{rev,C} - E_{rev,A})$ can be calculated by the Nernst equation, assuming a Nafion™ ionomer pH of 0: [25]

$$E_{rev,A(IOR)} = E^0 + \frac{RT}{zF} ln\left[\frac{a(ox)}{a(red)}\right] = 0.118\,V + \frac{RT}{zF} ln\left(\frac{[ACE]}{[IPA]}\right) \quad (1)$$

where R is the gas constant (8.314 J $molK^{-1}$), T is the temperature in Kelvin, $z(z_{IOR} = 2)$ is the electrochemical equivalent number, F is the Faraday constant (96485 C mol^{-1}), and $a(ox/red)$ are the activities for the oxidative and reductive species, respectively. $E_{rev,C}$ can be calculated accordingly as ORR for the DIFC or HER for the EDU.

3. MEA voltage contributions

The measured cell potential E_{cell} is a sum of many losses to the E_{rev}, whereas $E_{cell} < E_{rev}$ for galvanic cells (H_2PEMFC and DIFC) and $E_{cell} > E_{rev}$ for electrolytic cells (EDU) upon polarization: [41,42].

$$E_{cell} = E_{rev} \pm \left[\eta_A + \eta_C + \eta_{mt} + j\left(R_M + R_{el} + R^{eff}_{ion,A} + R^{eff}_{ion,C}\right)\right] \quad (2)$$

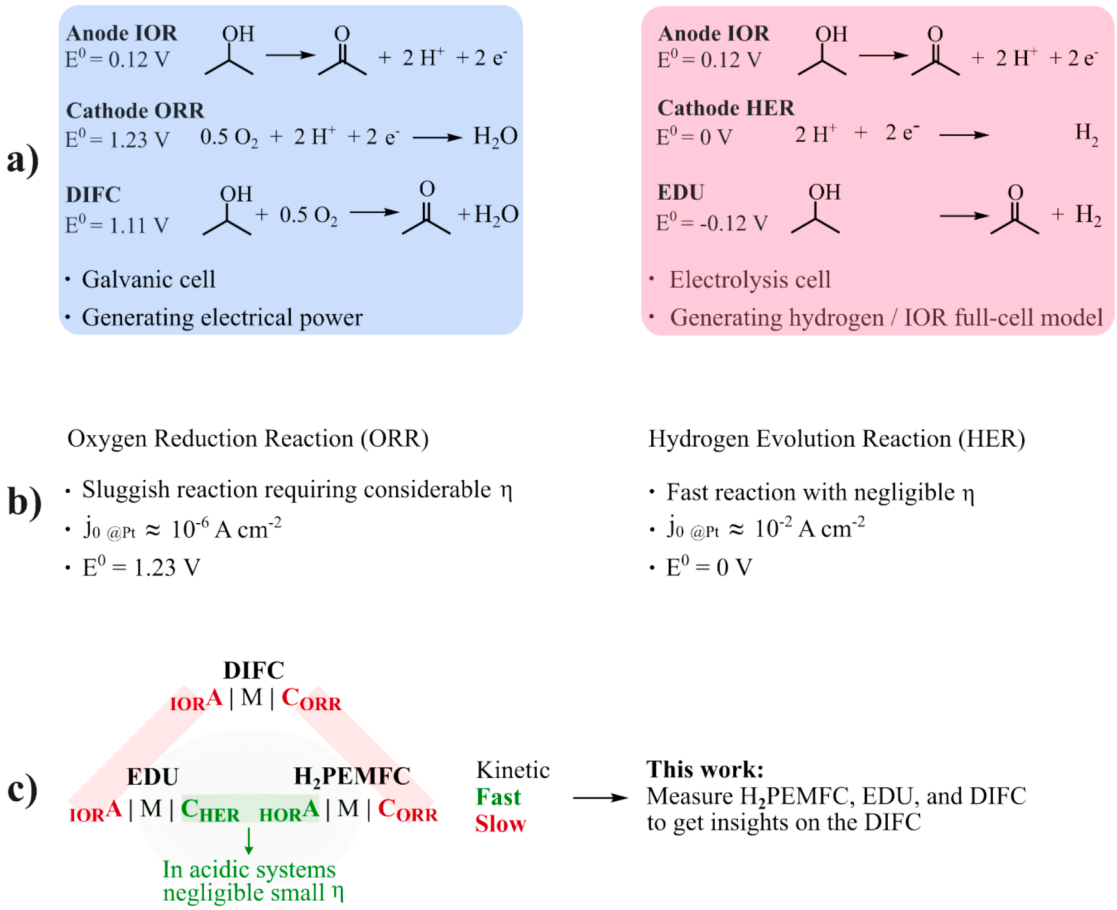

Fig. 3. (a) Comparison of the difc to the edu with the corresponding reaction equations. (b) Reaction characteristics of the cathodic reactions in the DIFC and EDU, respectively. (c) Concept of work: Deconstruction of the DIFC (two slow reactions) using the EDU and H_2PEMFC (each one negligible fast reaction). Fast and slow reactions are defined by their overpotential (η) at a given reaction rate and high exchange current densities (j_0) [2,3].

where η_A and η_C are the absolute values of the anodic and cathodic overpotentials at a given reaction rate, η_{mt} comprises mass transport losses, j is the cell's current, R_M and R_{el} are ohmic contributions of the membrane and electrical contact resistances, and $R^{eff}_{ion,A}$ and $R^{eff}_{ion,C}$ represent ion transport resistances in the anode and cathode catalyst layers, respectively.

E_{rev} can be calculated based on Eq. (1) and R_M and R_{el} can be determined as high-frequency resistance (HFR) via electrochemical impedance spectroscopy (EIS). Unfortunately, there are currently no accepted measurement techniques to quantify $R^{eff}_{ion,A}$, $R^{eff}_{ion,C}$, and η_{mt} for the ACE/IPA system. To quantify effective ion transport resistances in the catalyst layer, it is necessary to know the catalyst utilization for the IOR at PtRu, which is still unknown.

At low current densities, however, E_{cell} is mainly defined by E_{rev}, η_A, and η_C:

$$E_{cell@low\,j} \approx E_{rev} \pm (\eta_A + \eta_C) \tag{3}$$

Adding the HFR to Eq. (3) yields a refined expression for E_{cell} including four ascertainable parameters but η_A and η_C:

$$E_{cell@low\,j} \approx E_{rev} \pm [\eta_A + \eta_C + j{\cdot}\mathrm{HFR}] \tag{4}$$

Hence, at low current densities, it is sufficient to determine one of the two overpotentials to draw conclusions about the other.

3.1. Apparent IOR and ORR overpotentials

The HOR and HER at Pt in acidic environments are among the fastest known electrochemical reactions with negligibly small overpotentials [24,25]. Therefore, the H_2PEMFC is limited by the ORR, while the IOR limits the EDU.

Considering Eq. (4), at low current densities and negligibly overpotentials for the HOR and HER ($\eta_{HOR@Pt,acidic} = \eta_{HER@Pt,acidic} \approx 0$ V, Eq. (5)) [25], $\eta_{ORR|H_2FC}$ and $\eta_{IOR|EDU}$ are determinable by Eqs. (6) and (7).

η_{DIFC}, on the other hand, is a sum of two non-negligible overpotentials, the $\eta_{IOR|DIFC}$ and $\eta_{ORR|DIFC}$ (Eq. (8)). Nevertheless, when using the same MEA within the same setup using the same feed at the same temperature as DIFC and EDU, $\eta_{IOR|EDU}$ should be equal to $\eta_{IOR|DIFC}$ (Eq. (9)). Thereof, $\eta_{ORR|DIFC}$ is accessible via η_{DIFC} and $\eta_{IOR|EDU}$ (Eq. (10)).

$$\eta_{HOR@Pt,\,H^+} = \eta_{HER@Pt,\,H^+} \approx 0 \tag{5}$$

$$\eta_{H_2PEMFC} = \eta_{HOR|H_2PEMFC} + \eta_{ORR|H_2PEMFC} \approx \eta_{ORR|H_2PEMFC} \tag{6}$$

$$\eta_{EDU} = \eta_{IOR|EDU} + \eta_{HER|EDU} \approx \eta_{IOR|EDU} \tag{7}$$

$$\eta_{DIFC} = \eta_{IOR|DIFC} + \eta_{ORR|DIFC} \tag{8}$$

$$\eta_{IOR|EDU} \approx \eta_{IOR|DIFC} \tag{9}$$

$$\eta_{ORR|DIFC} \approx \eta_{DIFC} - \eta_{IOR|EDU} \tag{10}$$

Inserting Eqs. (6), (7), and (10) into Eq. (4) yields experimentally determinable expressions for the IOR and ORR overpotentials:

$$\eta_{ORR|H_2PEMFC} \approx E_{Rev|H_2PEMFC} - E_{cell|H_2FC} - j{\cdot}HFR_{H_2PEMFC} \tag{11}$$

$$\eta_{IOR|EDU} \approx E_{cell|EDU} - E_{Rev|EDU} - j{\cdot}HFR_{EDU} \quad (12)$$

$$\eta_{DIFC} \approx E_{Rev|DIFC} - E_{cell|DIFC} - j{\cdot}HFR_{DIFC} \quad (13)$$

$$\eta_{ORR|DIFC} \approx \eta_{DIFC} - \eta_{IOR|EDU} \quad (14)$$

Finally, comparing $\eta_{ORR|H_2FC}$ and $\eta_{ORR|DIFC}$ to the Butler Volmer equation using the Tafel approximation for the ORR ($\eta_{ORR,BV|Tafel}$) provides conclusions about the voltage losses that stem from fuel crossover, particularly the ACE/IPA crossover for the DIFC.

Because Eqs. (11), (12), and (14) use approximations, the corresponding overpotentials will be called apparent overpotentials in the following text.

3.2. Stable hydrogen reference potential

The E^0 of the HOR and HER at pH 0 is 0 V. However, this is only applicable for standard conditions, including a hydrogen partial pressure (p_{H_2}) of unity. Hence, a stable hydrogen partial pressure is a prerequisite for a stable hydrogen reference potential in order to investigate the reaction rate-limiting IOR in the EDU. During EDU operation, however, the cathodic HER would not be sufficient to generate a constant cathodic p_{H_2} at low current densities without an active hydrogen supply. Consequently, the cathodic potential would shift during operation, rendering the EDU polarization curves meaningless. This problem can be solved by constantly feeding the cathode with hydrogen, which ensures a stable cathode potential. In order to minimize the possible impact of hydrogen crossover, this work refrains from using a pure hydrogen supply for the EDU but instead fed a diluted 5 vol% H_2 reforming gas. This causes a Nernst shift of the cathodic potential:

$$E_{EDU,\,cathode} = E^0 + \frac{RT}{zF} ln\left[\frac{a(ox)}{a(red)}\right] = 0\,V + \frac{RT}{zF} ln\left[\frac{1}{p_{H_2}}\right] = -46\,mV \quad (15)$$

where E^0 is the standard potential for the HER and z ($z_{H_2} = 2$) is the electrochemical equivalent number. Because the HER increases the p_{H_2} during the experiment, a high flow rate of 1 L min^{-1} was chosen for the reforming gas flow rate to limit the maximum potential offset caused by the HER to $\Delta E = 1.2$ mV according to the maximum EDU current density. Consequently, the cathode potential can be considered a stable reference potential during OCV and cell operation (detailed calculations are in the supporting information section S1).

4. Experimental

4.1. Membrane electrode assembly manufacturing

Pre-dried (12 h at 150 °C, <10^{-5} bar) PtRu/C (40/20 wt%, HiSPEC 10,000, *Alfa Aesar*, USA) or Pt/C (38 wt%, TEC10V40E, *Tanaka*, Japan) were added to a 15 mL high-density polyethylene (HDPE) bottle containing 18 g of 5 mm diameter ZrO_2 grinding beads. 1-propanol (≥99.9 %, *Merck KGaA*, Germany) was then added under argon (5.0, *Air Liquide*, France) atmosphere (O_2 < 4 %). Afterward, water (18.2 MΩ, *Merck-MilliPore*, Germany) and Nafion™ D2021 (*Chemours*, USA) were added to either obtain a 10.8 wt% solid content PtRu ink with an ionomer to carbon ratio (I/C) of unity and a water/solvent ratio of 9.3 wt% or a 13.5 wt% solid content Pt ink with an I/C of 0.63 and a water/solvent ratio of 9.3 wt%. The inks were dispersed by a roller mill at 60 rpm for 20 h at ambient conditions. Then, the inks were cast onto a virgin PTFE substrate sheet (*High-tech-flon*®, Germany) and coated with 20 mm s^{-1} speed using the Meyer rod technique with a 120 µm rod for the PtRu ink or a 100 µm rod for the Pt ink and dried at ambient conditions, followed by drying at 70 °C.

To form the catalyst-coated membranes (CCM), 5 cm^{-2} electrodes were hot-pressed onto a Nafion™ XL membrane (*Chemours*, USA) using a Labline P200S hot-press (*COLLIN Lab & Pilot Solutions GmbH*, Germany) at a) 120 °C and 20 kPa cm^{-2} for 1 min, followed by a temperature and pressure ramp within 2.5 min to b) 155 °C and 500 kPa cm^{-2} for 4 min. The weight difference of the PTFE substrates with and without the catalyst layer determined the electrode loadings yielding 0.52 ± 0.009 mg_{PtRu} cm^{-2} for the anodes and 0.29 ± 0.017 mg_{Pt} cm^{-2} for the cathodes.

The CCMs were assembled with H23C2 gas diffusion layers (GDL) (*Freudenberg & Co. KG*, Germany) for the anode and H23C8 for the cathode to form membrane electrode assemblies (MEA).

4.2. MEA testing equipment

The MEA tests were performed using a Scribner® (*Scribner Associates Inc*, USA) 850e test bench, including a Scribner® cell fixture with 5 cm^2 single serpentine graphite flow fields. The cell fixtures were tightened using 5 Nm torque and glass fiber reinforced PTFE gaskets (*High-tech-flon*®, Germany), yielding a GDL compression of 20–25 %. A Masterflex® L/S peristaltic pump (*Cole-Parmer*®, USA) fed the cell with the organic reactant solutions. A VSP300 potentiostat (*Biologic*, France) was used to control the electrochemical measurements.

4.3. MEA electrochemical measurements

The MEA test protocol can be subdivided into three main parts (Fig. 1): H_2PEMFC, DIFC, and EDU. To compare the DIFC and EDU in the best possible way, the MEAs were conditioned as H_2PEMFC. Moreover, to eliminate the possible influence of sample history, three independently measured MEAs were tested in the sequence: H_2PEMFC, DIFC, and EDU. Three other independently measured MEAs were tested in the sequence: H_2PEMFC, EDU, and DIFC.

H_2PEMFC, DIFC, and EDU tests were performed at 60 °C, atmospheric pressure, and a cathode flow rate (Q_C) of 1 L min^{-1} at 97 % relative humidity (RH). For the H_2PEMFC and DIFC Q_C, synthetic air (SA) (5.0, *Air Liquide*, France) was used, while 5 % H_2 in N_2 (5.0, *Air Liquide*, France) was used for the EDU Q_C. The Q_A was 5 mL min^{-1} of the aqueous ACE/IPA for the DIFC and EDU, while 250 mL min^{-1} H_2 (5.0, *Air Liquide*, France) at 97 % RH was used for the H_2PEMFC. All flow rates represent highly over-stoichiometric flow rates to rule out fuel depletion (Fig. 4).

H_2PEMFC protocol: All MEAs were conditioned using a voltage-controlled sequence starting with 0.6 V for 35 min, 0.3 V for 10 min, OCV for 5 min, and 0.8 V for 10 min. This sequence was repeated 10 times, yielding constant performance. Ultimately, a 0.75 V hold for 15 min was conducted. Subsequently, the H_2PEMFC polarization characteristics were obtained using a galvanostatic protocol at 0, 1, 5, 10, 20, 40, 60, 80, 100, 120, 140, 160, 180, 200, 400, 600, 800, 1000, 1200, and 1400 mA cm^{-2}.

Hydrogen crossover and ohmic short measurements were performed in an N_2/H_2 environment (250 mL min^{-1} N_2, 250 mL min^{-1} H_2, both 97 % RH at 60 °C and atmospheric pressure) via voltage stepping (0.2 V–0.6 V in 0.1 V steps, holding time 2 min, and averaging the last 30 s)

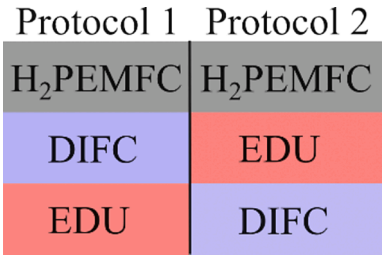

Fig. 4. MEA test sequence with six independently measured MEAs (3× protocol 1, 3× protocol 2). The hydrogen fuel cell measurements include a conditioning step, hydrogen crossover, and short measurements to ensure pristine and intact MEAs.

and linear sweep voltammetry (LSV) scans to obtain the hydrogen oxidation onset potential (0 V vs. OCV to 0.6 V at a scan rate of 2 mV s^{-1}).[43] Linear regression of the voltage stepping was performed, and the intercept with the onset potential was used to obtain the H_2 crossover values. The slope of the linear regression determines the inverse of the electric short.

DIFC and EDU protocol: To ensure pristine MEA states before each new set of experiments, the anode compartment was flushed with MiliQ water for at least 20 min with 5 mL min^{-1} before each new experiment. The DIFC and EDU polarization characteristics were obtained using a mixed galvanostatic and potentiostatic protocol. The low current density regime of 1–10 mA cm^{-2} was recorded galvanostatically. Because the catalyst's activity is potential dependent, higher current densities were recorded potentiostatically to avoid side reactions. The potentiostatic polarization curve points for the DIFC were at 700, 650, 600, 550, 500, 450, 400, 350, 300, 250, and 200 mV. The potentiostatic polarization curve points for the EDU were at 50, 75, 100, 125, 150, 175, 200, 250, 300, 350, 400 and 450 mV.

Each polarization point for H_2PEMFC, DIFC, and EDU was held for two minutes, while the last 30 s of each point were averaged for the data evaluation. Electrochemical impedance spectroscopy (EIS) was measured for each polarization point from 100 kHz to 10 Hz with 10–20 % perturbation for the galvanostatic protocols and 3 mV perturbation for the potentiostatic protocols to determine the high-frequency resistances (HFR) using an equivalent circuit (inductor + resistor) with a charge transfer transmission line model [44]. All impedance spectra were fitted using the impedance.py library [45].

Representative EIS raw data for the DIFC and EDU is given in the supporting information in section S2.

4.4. RDE sample preparation

A PTFE-supported glassy carbon (GC) electrode (5 mm diameter, *Pine Research*, USA) was polished with a 0.05 μm Al_2O_3 suspension (*Allied High Tech Products Inc*, USA) and cleaned by sonicating via a sonic bath (*VWR® USC*, USA) at low power in MiliQ water for 10 min, dipping in 5 M KOH (semiconductor grade, *Sigma Aldrich*, Germany) for >15 min, 3x dipping in MiliQ water each for >15 min, dipping in 1 M H_2SO_4 (Suprapur®, *Sigma Aldrich*, Germany) for >15 min, and 3x dipping in MiliQ water each for >15 min.

The corresponding Pt/C inks were prepared by adding MiliQ water and 2-propanol (≥99.9 %, *Merck KGaA*, Germany) to a pre-dried (120 °C, 40 mbar, 24 h) Pt/C catalyst powder (38 wt%, TEC10V40E, *Tanaka*, Japan). The suspension was dispersed 2x 15 min in a sonic bath at high power in ice-cold water. Subsequently, Nafion™ D520 (*Chemours*, USA) was added to the suspension, and the catalyst ink was dispersed for 15 min in a sonic bath at low power in ice-cold water.

The RDE Pt/C ink consisted of a solid content of 0.046 w%, an I/C of 0.2, and 30 v% IPA concentration corresponding to a loading of 14 μg_{Pt} cm^{-2} for 7.5 μL ink. After slowly warming the ink to room temperature, 7.5 μL Pt/C ink was drop-casted on the GC, covered by a small 3D-printed cylinder with a gas connection, and left to dry at room temperature under a constant low argon flow (5.0, *Air Liquide*, France).

4.5. RDE testing equipment

The RDE setup consists of a glass cell, a rotator, a GC working electrode, a Pt wire counter electrode (99.99 %) (all *Pine Research*, USA), a reversible hydrogen reference electrode (RHE Hydroflex, *Gaskatel*, Germany), a potentiostat (*Nordic Electrochemistry*, ECi 210, Denmark), and a chiller (±0.1 °C, *Huber*, Germany) to maintain controlled 30 °C throughout the measurements.

4.6. RDE electrochemical measurements

The RDE test protocol investigates the influence of ACE/IPA on the ORR (Fig. 2). The protocols start with a catalyst cleaning by cycling the potential 25x between 0.05–1.1 V_{RHE} at 50 mV s^{-1} (CV Cleaning) in an Ar-saturated 0.1 M H_2SO_4 electrolyte solution. Afterward, the electrolyte was renewed and Ar-saturated to record the hydrogen-under-potential-deposition (HUPD) by cycling the potential between 0.05–1.1 V_{RHE} each 3x at 5, 50, and 100 mV s^{-1} (CV HUPD) and to determine the resistance by EIS from 10 kHz–10 Hz at 0.2 V_{RHE} with an amplitude of 20 mV. After O_2-saturating the electrolyte, LSV ORR beginning-of-test polarization curves (LSV ORR BOT) were recorded 3x at 5 mV s^{-1} from 1.1–0.1 V_{RHE}. The electrolyte was replaced by 0.1 M H_2SO_4 solutions with either 25 mM acetone or isopropanol, then O_2-saturated, and finally, 3x LSV polarization curves were performed at 5 mV s^{-1} from 1.1–0.1 V_{RHE} (LSV ORR 25 mM ACE/IPA). This procedure was repeated with 0.1 M H_2SO_4 solutions with 50 mM acetone or isopropanol (LSV ORR 50 mM ACE/IPA). Finally, end-end-of-test ORR polarization curves in 0.1 M H_2SO_4 without acetone or isopropanol were recorded (LSV ORR EOT).

All measurements were performed at 30 °C, and all CV and LSV were measured at 1600 rpm rotation speed. The third scan of every ORR polarization is used for data evaluation. The acetone and isopropanol measurements were performed at different tip-coated electrodes (Fig. 5).

5. Results and discussion

5.1. DIFC and EDU polarization curves

Fig. 6 depicts (a) the DIFC and (b) EDU polarization curves at 60 °C and varying ACE/IPA ratios with a total organic concentration of 1 M. Both DIFC and EDU curves are dominated by the early IOR peak at PtRu: The DIFC shows the characteristic peak at 0.6 V, lower voltage leads to lower current densities. Contrarily, the EDU shows the characteristic peak at 0.1 V, which means that higher voltages cause lower current densities. In addition, the polarization curves exhibit the beginning of the second IOR peak at low DIFC and high EDU voltages. Further increasing the anode potential is avoided to prevent Ru oxidation [46].

The EDU represents the anode of the DIFC in an electrolytic MEA cell. The curves must be read accordingly: The DIFC (galvanic cell) should have a high voltage for a given reaction rate, whereas the EDU (electrolytic cell) should have a low voltage for a given reaction rate. Due to convention, current and potential are both plotted positively for the DIFC and EDU. The E_{calc} EDU y-axis is the voltage corrected to 100 % H_2, accounting for the −46 mV Nerstian shift caused by the 5 % H_2 feed, according to equation (15) (details in the SI section S1).

In accordance to equation (1), $E_{rev,IOR}$ increases with increasing acetone concentration, yielding downshifted polarization curves for the DIFC, while upshifted polarization curves for the EDU when changing the acetone feed concentration from 0.95 M IPA/0.05 M ACE to 0.75 M IPA/0.25 M ACE. Furthermore, the peak current densities for the DIFC and EDU are strongly dependent on the ACE/IPA reaction equilibrium, too. The higher the isopropanol concentration (reactant), the higher the reaction rate. Increasing the acetone (product) feed concentration from

Protocol 1	Protocol 2
CV Cleaning	CV Cleaning
CV HUPD	CV HUPD
EIS	EIS
LSV ORR BOT	LSV ORR BOT
LSV ORR 25 mM Ace	LSV ORR 25 mM Ipa
LSV ORR 50 mM Ace	LSV ORR 50 mM Ipa
LSV ORR EOT	LSV ORR EOT

Fig. 5. RDE test sequence for independently measured Pt/C GC electrodes at 30 °C in either O_2 saturated (ORR) or Ar saturated (rest) 0.1 M H_2SO_4 solutions.

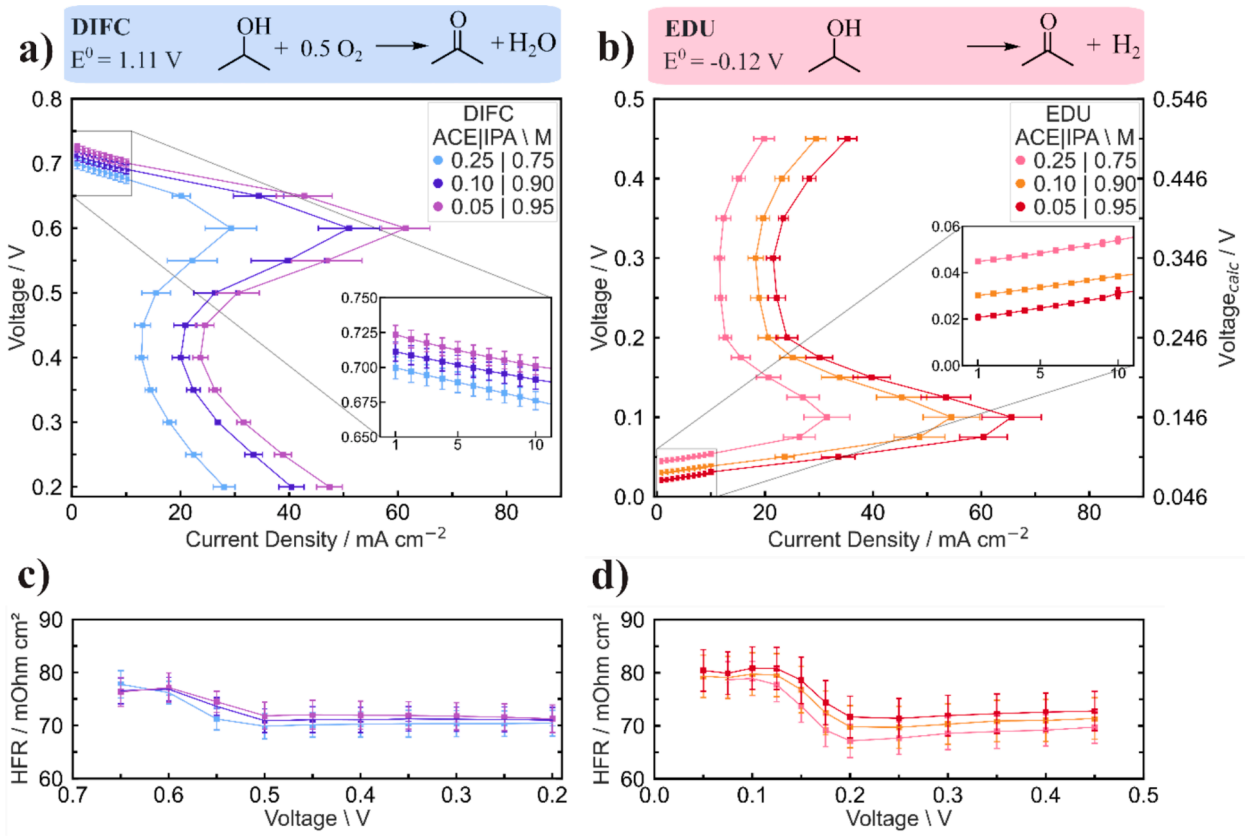

Fig. 6. Polarization curves at varying ACE/IPA ratios at 60 °C for (a) DIFC and (b) EDU. The E_{calc} EDU y-axis is the voltage corrected to 100 % H_2, accounting for the Nerstian shift caused by the 5 % H_2 feed, according to equation (15). The polarization data points represent the average of the last 30 s of a 2-min hold. HFR values are given for (c) DIFC and (d) EDU. The error bars represent the standard deviation of six independently measured MEAs.

0.95 M IPA/0.05 M ACE to 0.75 M IPA/0.25 M ACE leads to a peak current density drop from 62 mA cm^{-2} to 28 mA cm^{-2} for the DIFC and a peak current density drop from 65 mA cm^{-2} to 31 mA cm^{-2} for the EDU. The almost equal current densities for the DIFC and EDU show that both systems are rate-limited by the IOR, confirming the EDU as an IOR full-cell model of the DIFC.

The HFR values show neither considerable differences between the DIFC and EDU nor the ACE/IPA ratios. Higher current densities lead to a slightly lower HFR correlated to a higher osmotic drag and, therefore, better membrane humidification.

The H_2PEMFC OCV of the investigated MEAs is 994 ± 5 mV, representing the average of the last 30 s of a 5 min OCV hold. The normal H_2PEMFC OCV indicates the integrity of the tested MEAs. The H_2PEMFC polarization curves, HFR values, and hydrogen crossover results are given in the supporting information section S3.

5.2. DIFC and EDU OCV

The high OCV is one of the most important advantages of the DIFC compared to other DAFCs. Surprisingly, the DIFC does not have the highest E_{rev}. [3] Hence, if the thermodynamics of the involved reactions cannot explain this OCV, there must be a correlation to the fuel crossover. Consequently, the DIFC exhibits either lower fuel crossover than other DAFCs when using Nafion™ membranes or smaller effects of the internal currents caused by the fuel crossover.

Santasalo et al. [11] suspect the IOR kinetic to be comparable fast, causing smaller effects of the crossover on the DIFC. *Godino et al.* [47] revealed an equally high permeability of 1-propanol and isopropanol, which is 50 % higher than methanol at 20 wt% alcohol concentrations through a Nafion™ 117 membrane.

Considering the low 1-propanol fuel cell OCV (Fig. 1) at similar alcohol permeability of 1-propanol and isopropanol and the low DMFC OCV at lower alcohol permeability of methanol compared to isopropanol, the high DIFC OCV can not be justified by the amount of fuel crossover alone.

(OCV: DIFC > DMFC > 1-Prop-FC; fuel permeability: IPA ≈ 1-Prop ≫ MeOH)

Thus, the effects of the internal currents remain the likely cause of the high DIFC OCV. While the cell is at OCV, no external current flows through the circuit. Nevertheless, internal currents at the individual electrodes can still occur. Internal currents mainly correspond to oxidative and reductive reactions at each electrode caused by fuel crossover, yielding a mixed potential loss, whereby the kinetics of the involved reactions describe the extent of the losses [16,17]. That means faster reactions exhibit relatively lower OCV losses at a given crossover rate. Additionally, electric short currents through the membrane can cause OCV losses. However, they cannot explain the general difference between the DIFC and other DAFC OCVs.

For the DIFC and EDU experiments, the same MEAs within the same setup were used with the same feed at the same temperature. Thus, the ACE/IPA crossover is expected to be the same for the DIFC and EDU. If the kinetics of the involved reactions influence the OCV at a given crossover rate, there should be a difference in OCV losses for the DIFC and EDU.

Fig. 7a illustrates this difference in OCV loss between the DIFC and EDU. The DIFC exhibits OCV values in an expected range. Nevertheless, these values correspond to a considerable OCV loss to E_{rev}. The EDU, in contrast, reveals almost no OCV loss, nearly matching the thermodynamic E_{rev}. Furthermore, the DIFC OCV drops with increasing acetone concentrations, while the EDU OCV rises with increasing acetone concentrations, following the thermodynamically predicted trends given by

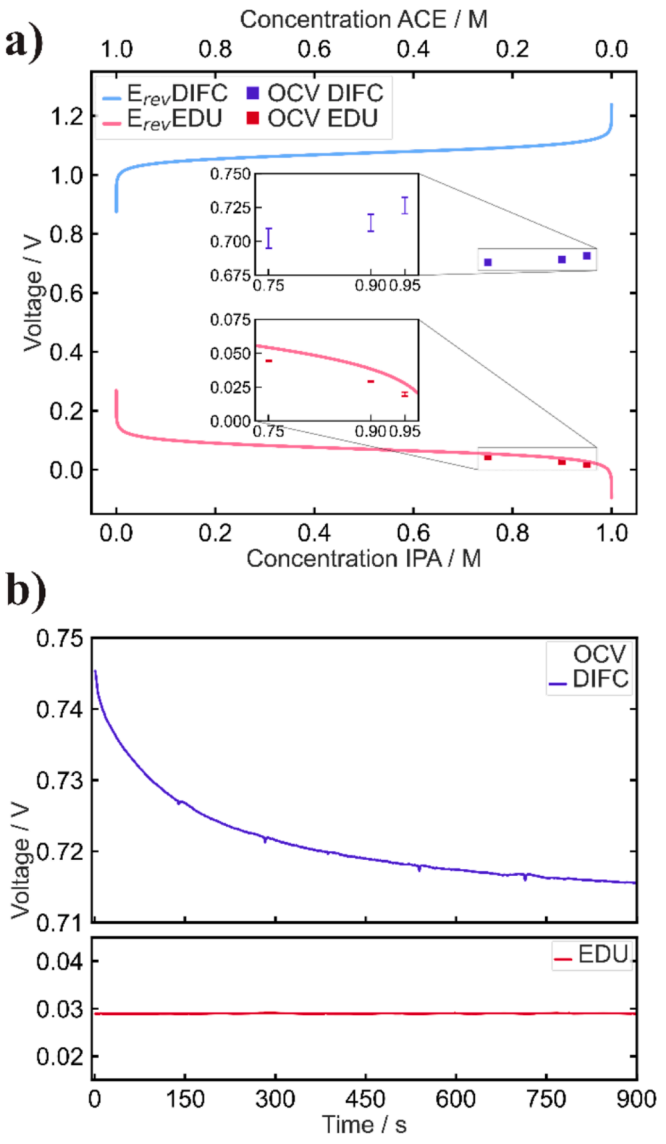

Fig. 7. (a) E_{rev} and OCV for the DIFC (blue) and EDU (red) at varying ACE/IPA rations with a total organic concentration of 1 M at 60 °C. E_{rev} calculated according to equation (1) with limit concentration ratios of 1^{-5} M and 0.99999 M of ACE/IPA and IPA/ACE, respectively, to indicate the curve behavior, but omitting theoretical limit values of $\pm\infty$ V at 0 M and 1 M. The data points represent the average of the last 30 s of a 15-minute OCV hold. The error bars represent the standard deviation of six independently measured MEAs. (b) Representative raw data of a 15 min OCV hold for the DIFC(blue) and the EDU (red) using 0.9 M IPA| 0.1 M ACE at 60 °C.

(1).

The distinct differences in OCV losses for the DIFC and EDU must be explained, along with the influence of the ACE/IPA crossover on the different cathodic reactions. For the DIFC, when isopropanol crosses the membrane, it meets a Pt-cathode at low pH with a theoretical potential of 1.19 V ($E_{rev,ORR}$ at 60 °C, SA at 97 % RH, and atmospheric pressure). This potential is very high compared to the $E_{rev,IOR}$, and is likely to promote an electrochemical oxidation of isopropanol. In contrast, for the EDU, when isopropanol crosses the membrane, it meets a Pt cathode at low pH and a theoretical potential of −0.046 V ($E_{rev,HER}$ at 60 °C, 5 % H_2 in N_2 at 97 % RH, and atmospheric pressure), which does not lead to an oxidation of isopropanol.

That means the EDU OCV remains unaffected by ACE/IPA crossover, whereas, for the DIFC OCV, the crossover can be oxidized, yielding mixed potentials and leading to noticeable OCV losses.

In addition, Fig. 7b displays the DIFC and EDU OCV as a function of time within a 15 min hold. While the DIFC OCV constantly decays over time, the EDU OCV stays constant. It reflects how the HER in the EDU is unaffected by the ACE/IPA crossover and how it affects the ORR in the DIFC.

The small EDU OCV losses not only indicate that the cathodic HER is unaffected by ACE/IPA but also that the anodic IOR is barely affected by hydrogen crossover or dissolved oxygen of the feed solutions (the EDU anode will inevitably be subjected to dissolved oxygen in the aqueous ACE/IPA solutions due to the sample preparation, which occurred under atmospheric conditions). This result suggests fast kinetics for the IOR and HER, compared to the oxidation of primary alcohols, which aligns with *Santasalo et al.*'s [11] earlier assumption. Finally, a relatively fast IOR could explain the exceptionally high OCV of the DIFC. Further information on the apparent overpotential for the IOR will follow later in the text.

5.3. Influence of ACE/IPA on the ORR

To further investigate the influence of ACE/IPA on the ORR in a DIFC, RDE polarization curves were performed at Pt in O_2-saturated 0.1 M H_2SO_4 at 30 °C with and without ACE/IPA mimicking crossover in a DIFC. The expected negative effects include reduced ORR activity, an oxidative shift due to ACE/IPA oxidation, and a lower limiting current density due to possible Pt surface coverage.

Fig. 8a shows a relatively small influence of acetone on the ORR. The ORR onset potential is not shifted, the ORR activity is slightly reduced between 0.8 and 0.6 V_{RHE}, and the limiting current density is barely influenced. However, these minor influences scale with the concentration of acetone. For the 50 mM experiment, the effects are more pronounced than those of the 25 mM experiment. The results indicate that the acetone crossover in a DIFC does not lead to considerable OCV losses.

In contrast, Fig. 8b displays a clear influence of isopropanol on the ORR activity that also scales with the isopropanol concentration. At around 1 V_{RHE}, the curve is slightly shifted oxidatively, indicating an isopropanol oxidation. Moreover, at 0.6 V_{RHE}, the curve exhibits an oxidative peak, significantly reducing the overall reductive current. This peak coincides with the IOR peak at Pt [4,5,48]. That means the ORR is rivaling the IOR, strongly impairing the target reaction. This evidence confirms the earlier argument the isopropanol crossover in a DIFC strongly influences the DIFC cathode. The higher the isopropanol crossover, the higher the OCV losses for the DIFC.

The ACE/IPA concentrations used here show the qualitative influence of crossover on the DIFC. However, they are not a quantitative representation. The actual DIFC crossover is a function of the ACE/IPA concentration, temperature, membrane (integrity), and current density.

The beginning of test (BOT) and end of test (EOT) measurements show the reversibility of the ACE/IPA influence on the ORR. The initial ORR activity was restored after removing the ACE/IPA solutions.

RDE EIS, hydrogen under potential deposition CVs, and CV scans of Ar-saturated 0.1 M H_2SO_4 with 50 mM ACE/IPA at 30 °C confirming acetone being not oxidized within 0.05–1.1 V_{RHE}, are given in the supporting information section S4.

5.4. IOR and ORR overpotentials for the DIFC and EDU

Eqs. (11), (12), and (14) are applied within Fig. 9, depicting current densities as a function of the apparent overpotentials to get further information on the IOR and ORR in a DIFC. The characteristic IOR peak (Fig. 6) requires recording the DIFC and EDU polarization curves as a combined galvanostatic and potentiostatic protocol (Experimental). However, for potentiostatic protocols, one cannot predict the exact current response. Hence, to correlate DIFC and EDU current densities, the polarization curves were fitted using a polynomial function and interpolated to have a continuous mathematical description for the

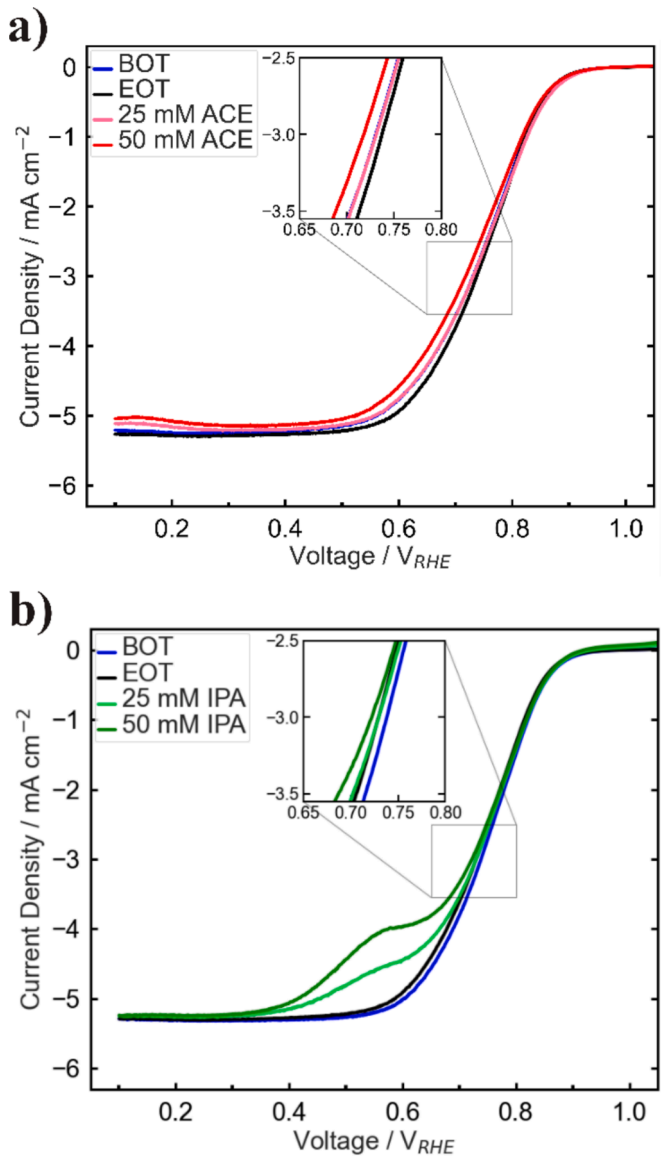

Fig. 8. RDE LSV scans (5 mV s^{-1}) in O_2-saturated 0.1 M H_2SO_4 at 30 °C and 1600 rpm rotation using 14 μg_{Pt} cm^{-2} (Pt/C) to compare the influence of (a) acetone and (b) isopropanol on the ORR. BOT and EOT represent the "beginning of test" and "end of test" measurements without ACE/IPA. The acetone and isopropanol measurements were performed at different tip-coated electrodes.

voltage as a function of the current density. These functions are used to interpolate between the potentiostatic polarization curve points and are a sole mathematical description, not based on a physical function.

For the solely kinetic description of the ORR, the Butler-Volmer equation with the Tafel approximation gives:

$\eta_{ORR|BV_{Tafel}} = \frac{RT}{\alpha n F} \ln \frac{j}{j_0}$ (16)α (=0.5) is the symmetry factor for the Butler–Volmer equation and j_0 is the exchange current density for the ORR [49]. The H_2PEMFC polarization curve was fitted according to Eq. (16) and the corresponding HFR. Information on the interpolated fit functions with the respective R^2 values are given in the supporting information section S5.

The apparent IOR overpotentials in Fig. 9(red) for 1–10 mA cm^{-2} are in the range of only 20 mV. Moreover, $\eta_{IOR|EDU}$ are in good agreement with each other for lower current densities. Overlapping $\eta_{IOR|EDU}$ at lower current densities for the different ACE/IPA ratios, correcting for E_{rev} and the HFR indicate that Eq. (11) is a good approximation.

Actually, $\eta_{IOR|EDU}$ is small compared to other alcohol oxidations in

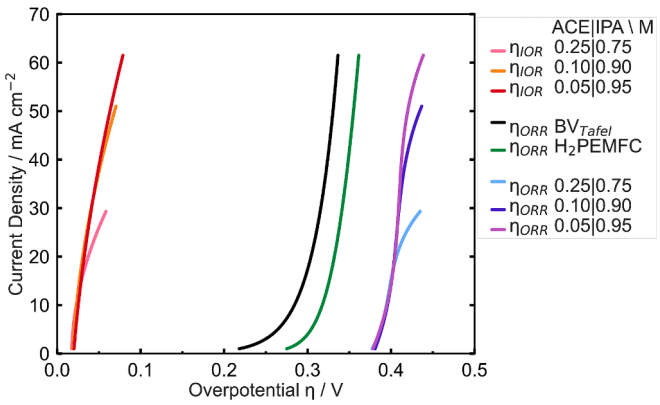

Fig. 9. IOR(red) and ORR(blue) overpotentials at 60 °C and 1–62 mA cm^{-2} or to the corresponding maximum current density for the H_2PEMFC, EDU, and DIFC according to (11), (12), (14), and the pure kinetic ORR overpotential according to the Butler-Volmer equation using the Tafel approximation(black). For equations (12) and (14), the current densities for the overpotential evaluation are limited to 1 mA cm^{-2} until the corresponding maximum current density, comprising the first peak IOR peak.

DAFCs. Depending on the literature source, the overpotential at 10 mA cm^{-2} is between 300–500 mV for the methanol oxidation reaction [50–54]. Although it is difficult to compare the results from different laboratories, the results of the methanol oxidation reaction are so significantly higher that a general difference between methanol oxidation and IOR can be assumed.

That indicates *Santasalo et al.*'s [11] earlier assumption is correct: The low $\eta_{IOR|EDU}$ is the likely reason for the high DIFC OCV. Despite a higher E_{rev} and a higher organics crossover for the DIFC compared to the DMFC, the small $\eta_{IOR|EDU}$ causing only minor anodic OCV losses and, thus, a relatively high DIFC OCV. Accordingly, the EDU combines a relatively fast IOR with the very fast HER, causing only minor OCV losses for both electrodes. Thus, the small $\eta_{IOR|EDU}$ also explains the hardly existing EDU OCV losses.

However, near the corresponding maximum EDU reaction rate, the apparent IOR overpotentials Fig. 9 (red) curves differ. It indicates that Eq. (12) is no longer a good approximation for reaction rates with higher overpotentials than the peak current density. The probable reason is acetone (product) accumulation in the catalyst layer, causing an unfavorable Nerstian shift and slow acetone desorption, which has already been described for the DIFC in the literature [3,5,23,55,56]. Slow product desorption leads to depletion of the active PtRu centers for the IOR and can, therefore, be assigned to the mass transport η_{MT} of Eq. (2). Therefore, the current densities for the overpotential evaluation are limited to 1 mA cm^{-2} until the corresponding maximum current density, comprising the first peak IOR peak.

Fig. 9 (black and green) shows the solely kinetic Butler–Volmer η_{ORR} and the apparent H_2PEMFC- and DIFC η_{ORR}. The Butler–Volmer Tafel approximation describes the lowest possible η_{ORR} without impairment. $\eta_{ORR|H_2PEMFC}$, in turn, is mainly impaired by the hydrogen crossover, causing noticeable cathodic OCV losses [16,17].

The apparent DIFC ORR overpotentials in Fig. 9(blue) for 1–10 mA cm^{-2} are in the range of 380 mV. Similar to the IOR, $\eta_{ORR|DIFC}$ are in good agreement with each other for the different ACE/IPA ratios for lower current densities, indicating that Eq. (14) is a good approximation.

$\eta_{ORR|DIFC}$ is high compared to both $\eta_{ORR|BV_{Tafel}}$ and $\eta_{ORR|H_2PEMFC}$. This result shows that the ACE/IPA crossover affects the DIFC cathode severely. The overpotential required to drive the reaction is so high that it could also explain why the DIFC polarization curves with Nafion™ membranes do not show an activation region. *Hauenstein et al.* [9] raised the question of why the DIFC does not show a steep decline for the low

current region like for H_2PEMFCs or predicted by the Butler Volmer equation for the ORR. The $\eta_{ORR|DIFC}$ might be already beyond the steep decline of the Butler-Volmer equation even at low net reaction rates, yielding a steady decline for the DIFC at low current densities.

Near the corresponding maximum DIFC reaction rate, the apparent $\eta_{ORR|DIFC}$ Fig. 9 curves differ. It indicates that Eq. (14) is no longer a good approximation for higher reaction rates. Higher current densities correspond to lower cathode potentials for the DIFC, which increases the IOR activity, according to Fig. 8, resulting in two rivaling reactions, whereby a high $\eta_{ORR|DIFC}$ has to be paid. Additionally, slow acetone desorption can also play a role, reducing the active PtRu centers. Therefore, the current densities for the overpotential evaluation are limited to 1 mA cm^{-2} until the corresponding maximum current density, comprising the first peak IOR peak. The results reveal how the ACE/IPA crossover impairs the DIFC cathode and demonstrate the upside capabilities of new membrane materials mitigating crossover or new ORR active catalysts that are inactive for the IOR.

It is important to note that the apparent DIFC ORR overpotentials are also a function of the ACE/IPA crossover. The crossover is a function of temperature, feed concentration, the integrity of the MEA, the membrane material, and the current density. Accordingly, the values are comparable to the EDU in the same setup. For a general classification, the $\eta_{ORR|DIFC}$ values are to be assessed qualitatively. The results presented here aim to show qualitatively how the ACE/IPA crossover influences the DIFC ORR and they give a range for the corresponding losses.

6. Conclusion

This work investigates characteristic features of the DIFC and demonstrates how the acetone and isopropanol crossover affect the cathode of a DIFC. The electrolytic EDU cell, consisting of the IOR and the kinetically fast HER in acidic media using a PEM, produces hydrogen upon polarization (Fig. 3, Ib). The EDU serves as an IOR full-cell model to get insights on the DIFC. Investigating the influence of different ACE/IPA (product/reactant) ratios on the DIFC and EDU polarization curves shows a strong dependence on this reaction equilibrium, whereby both systems are rate-limited by the IOR.

The EDU OCV is electrochemically almost unaffected by crossover and is very close to E_{rev} , while the DIFC exhibits considerable OCV losses. Low cathode potentials (EDU HER) prevent ACE/IPA crossover oxidation. In contrast, high cathode potentials (DIFC ORR) cause rivaling IOR and ORR, leading to cathodic DIFC OCV losses. While the DIFC OCV constantly decays over time, the EDU OCV stays constant. Furthermore, the DIFC OCV drops with increasing acetone concentrations, while the EDU OCV rises with increasing acetone concentrations, following the thermodynamically predicted trends.

RDE ORR experiments investigate the different impact of acetone and isopropanol on the ORR, mimicking the ACE/IPA fuel crossover in the DIFC. Acetone crossover hardly affects the ORR, whereas an isopropanol crossover is oxidized, impairing the ORR and causing the cathodic DIFC OCV losses.

Based on Eqs. (11), (12), and (14) apparent overpotentials for the IOR and ORR can be calculated, revealing comparable low $\eta_{IOR|EDU}$ at PtRu and considerably high $\eta_{ORR|DIFC}$.

Low $\eta_{IOR|EDU}$ confirms *Santasalo et al.*'s [11] earlier assumption to be correct: The low $\eta_{IOR|EDU}$ is the likely reason for the high DIFC OCV. Despite a higher E_{rev} and a higher organics crossover rates for the DIFC compared to the DMFC, the small $\eta_{IOR|EDU}$ causing only minor anodic OCV losses and, thus, a relatively high DIFC OCV. Accordingly, the small $\eta_{IOR|EDU}$ also explains the hardly existing EDU OCV losses. $\eta_{ORR|DIFC}$ is high compared to both $\eta_{ORR|BV_{Tafel}}$ and $\eta_{ORR|H_2PEMFC}$. This result shows that the ACE/IPA crossover affects the DIFC cathode severely. The overpotential required to drive the reaction is so high that it can also explain why the DIFC polarization curves with Nafion^{TM} membranes do not show an activation region.

Overall, this comparison study reveals how the ACE/IPA crossover impairs the DIFC cathode and demonstrates the upside capabilities of new membrane materials mitigating crossover or new ORR active catalysts that are inactive for the IOR. The EDU serves well as a full-cell IOR model with low OCV losses. Moreover, depending on the application, the EDU could also be a valuable and voltage-efficient part within an EC-LOHC hydrogen storage system, whereby the EDU can release hydrogen on demand from easily storable and rehydrogenable IPA.

Author contributions

D. Venus conceived the concept, performed all experiments, evaluated the data, and wrote the manuscript. M. Valeske conceived the RDE experiments and reviewed and revised the manuscript. M. Brodt reviewed and revised the manuscript. P. Wasserscheid reviewed and revised the manuscript and provided funding acquisition. S. Thiele reviewed and revised the manuscript, supervised the project, and provided funding acquisition. All the authors participated in the study discussion and approved the final version of the manuscript.

CRediT authorship contribution statement

Dominik Venus: . **Moritz Valeske:** Writing – review & editing. **Matthew Brodt:** Writing – review & editing, Supervision. **Peter Wasserscheid:** Writing – review & editing, Funding acquisition. **Simon Thiele:** Writing – review & editing, Visualization, Supervision, Project administration, Methodology, Funding acquisition.

Declaration of competing interest

The authors declare that they have no known competing financial interests or personal relationships that could have appeared to influence the work reported in this paper.

Acknowledgments

We gratefully acknowledge the Bavarian Ministry of Economic Affairs, Regional Development, and Energy for funding this work.

Appendix A. Supplementary data

Supplementary data to this article can be found online at https://doi.org/10.1016/j.elecom.2024.107823.

Data availability

Data will be made available on request.

References

[1] H.R. Corti, E.R. Gonzalez, Direct Alcohol Fuel Cells (2014), https://doi.org/10.1007/978-94-007-7708-8.
[2] E. Berretti, L. Osmieri, V. Baglio, H.A. Miller, J. Filippi, F. Vizza, M. Santamaria, S. Specchia, C. Santoro, A. Lavacchi, Direct alcohol fuel cells: a comparative review of acidic and alkaline systems, Electrochem. Energy Rev. 6 (2023), https://doi.org/10.1007/s41918-023-00189-3.
[3] M. Brodt, K. Müller, J. Kerres, I. Katsounaros, K. Mayrhofer, P. Preuster, P. Wasserscheid, S. Thiele, The 2-propanol fuel cell: a review from the perspective of a hydrogen energy economy, Energy Tech 9 (2021) 2100164, https://doi.org/10.1002/ente.202100164.
[4] I. Mangoufis-Giasin, O. Piqué, P. Khanipour, K.J. Mayrhofer, F. Calle-Vallejo, I. Katsounaros, Different promoting roles of ruthenium for the oxidation of primary and secondary alcohols on PtRu electrocatalysts, J. Catal. 400 (2021) 166–172, https://doi.org/10.1016/j.jcat.2021.05.028.
[5] P. Khanipour, F.D. Speck, I. Mangoufis-Giasin, K.J.J. Mayrhofer, S. Cherevko, I. Katsounaros, Electrochemical oxidation of isopropanol on platinum-ruthenium nanoparticles studied with real-time product and dissolution analytics, ACS Appl.

Mater. Interfaces 12 (2020) 33670–33678, https://doi.org/10.1021/acsami.0c07190.
[6] C.J. Bondue, Z. Liang, M.T.M. Koper, Dissociative adsorption of acetone on platinum single-crystal electrodes, J. Phys. Chem. C 125 (2021) 6643–6649, https://doi.org/10.1021/acs.jpcc.0c11360.
[7] Y. Ando, Y. Aoyama, T. Sasaki, Y. Saito, H. Hatori, T. Tanaka, Effect of catalytic and electrochemical acetone hydrogenation on the I-V characteristics of an acetone/hydrogen-based thermally regenerative fuel cell, BCSJ 77 (2004) 1855–1859, https://doi.org/10.1246/bcsj.77.1855.
[8] S.K. Green, G.A. Tompsett, H.J. Kim, W. Bae Kim, G.W. Huber, Electrocatalytic reduction of acetone in a proton-exchange-membrane reactor: a model reaction for the electrocatalytic reduction of biomass, ChemSusChem 5 (2012) 2410–2420, https://doi.org/10.1002/cssc.201200416.
[9] P. Hauenstein, D. Seeberger, P. Wasserscheid, S. Thiele, High performance direct organic fuel cell using the acetone/isopropanol liquid organic hydrogen carrier system, Electrochem. Commun. 118 (2020) 106786, https://doi.org/10.1016/j.elecom.2020.106786.
[10] L. Fusek, V. Briega-Martos, M. Minichová, L. Fromm, E. Franz, J. Yang, A. Görling, K.J.J. Mayrhofer, P. Wasserscheid, S. Cherevko, O. Brummel, J. Libuda, Toward high-energy-density fuels for direct liquid organic hydrogen carrier fuel cells: electrooxidation of 1-cyclohexylethanol, J. Phys. Chem. Lett. 15 (2024) 2529–2536, https://doi.org/10.1021/acs.jpclett.3c03331.
[11] B.A. Santasalo, T. Kallio, K. Kontturi, Performance of liquid fuels in a platinum-ruthenium-catalysed polymer electrolyte fuel cell, Platin Met Rev 53 (2009) 58–66, https://doi.org/10.1595/147106709X416040.
[12] Z. Qi, A. Kaufman, Performance of 2-propanol in direct-oxidation fuel cells, J. Power Sources 112 (2002) 121–129, https://doi.org/10.1016/S0378-7753(02)00357-9.
[13] Z. Qi, A. Kaufman, Open circuit voltage and methanol crossover in DMFCs, J. Power Sources 110 (2002) 177–185, https://doi.org/10.1016/S0378-7753(02)00268-9.
[14] S. Song, W. Zhou, J. Tian, G. Rui Cai, Q. Sun, S. Xin, P.T. Kontou, Ethanol crossover phenomena and its influence on the performance of DEFC, J. Power Sources 145 (2005) 266–271, https://doi.org/10.1016/j.jpowsour.2004.12.065.
[15] S. Auffarth, W. Dafinger, J. Mehler, V. Ardizzon, P. Preuster, P. Wasserscheid, S. Thiele, J. Kerres, Cross-linked proton-exchange membranes with strongly reduced fuel crossover and increased chemical stability for direct-isopropanol fuel cells, J. Mater. Chem. A 10 (2022) 17208–17216, https://doi.org/10.1039/D2TA03832C.
[16] S.A. Vilekar, R. Datta, The effect of hydrogen crossover on open-circuit voltage in polymer electrolyte membrane fuel cells, J. Power Sources 195 (2010) 2241–2247, https://doi.org/10.1016/j.jpowsour.2009.10.023.
[17] M. Moore, S. Shukla, S. Voss, K. Karan, A. Weber, I. Zenyuk, M. Secanell, A numerical study on the impact of cathode catalyst layer loading on the open circuit voltage in a proton exchange membrane fuel cell, J. Electrochem. Soc. 168 (2021) 44519, https://doi.org/10.1149/1945-7111/abf50c.
[18] National Institute of Standards and Technology, NIST: Isopropyl Alcohol, 2024. <https://webbook.nist.gov/cgi/cbook.cgi?ID=C67630&Mask=2#Thermo-Condensed> (Accessed 8 July 2024).
[19] National Institute of Standards and Technology, NIST:Acetone, 2023. <https://webbook.nist.gov/cgi/cbook.cgi?ID=C67641&Mask=2#Thermo-Condensed> (Accessed 26 July 2023).
[20] National Institute of Standards and Technology, Ethanol, NIST, 2024. <https://webbook.nist.gov/cgi/cbook.cgi?ID=C64175&Mask=1#Thermo-Gas> (Accessed 8 July 2024).
[21] National Institute of Standards and Technology, Methyl Alcohol, NIST, 2024. <https://webbook.nist.gov/cgi/cbook.cgi?ID=C67561&Mask=1#Thermo-Gas> (Accessed 8 July 2024).
[22] P. Khanipour, M. Löffler, A.M. Reichert, F.T. Haase, K.J.J. Mayrhofer, I. Katsounaros, Electrochemical Real-Time Mass Spectrometry (EC-RTMS): monitoring electrochemical reaction products in real time, Angew. Chem. Int. Ed Engl. 58 (2019) 7273–7277, https://doi.org/10.1002/anie.201901923.
[23] P. Hauenstein, I. Mangoufis-Giasin, D. Seeberger, P. Wasserscheid, K.J. Mayrhofer, I. Katsounaros, S. Thiele, Impact of catalyst loading, ionomer content, and carbon support on the performance of direct isopropanol fuel cells, J. Power Sources Adv. 10 (2021) 100064, https://doi.org/10.1016/j.powera.2021.100064.
[24] K.C. Neyerlin, Gu. Wenbin, J. Jorne, H.A. Gasteiger, Study of the exchange current density for the hydrogen oxidation and evolution reactions, J. Electrochem. Soc. 154 (2007) 631.635, https://doi.org/10.1149/1.2733987.
[25] J. Durst, A. Siebel, C. Simon, F. Hasche, J. Herranz, H.A. Gasteiger, New insights into the electrochemical hydrogen oxidation and evolution reaction mechanism, Energy Environ. Sci. 7 (2014) 2255, https://doi.org/10.1039/C4EE00440J.
[26] C. Lamy, B. Guenot, M. Cretin, G. Pourcelly, Kinetics analysis of the electrocatalytic oxidation of methanol inside a DMFC working as a PEM Electrolysis Cell (PEMEC) to generate clean hydrogen, Electrochim. Acta 177 (2015) 352–358, https://doi.org/10.1016/j.electacta.2015.02.069.
[27] F.M. Sapountzi, M.N. Tsampas, H. Fredriksson, J.M. Gracia, J.W. Niemantsverdriet, Hydrogen from electrochemical reforming of C1–C3 alcohols using proton conducting membranes, Int. J. Hydrogen Energy 42 (2017) 10762–10774, https://doi.org/10.1016/j.ijhydene.2017.02.195.
[28] B. Hasa, J. Vakros, A. Katsaounis, Study of low temperatur electro reforming of EthOh and MeOH, Mater. Today (2018) 27337–27344, https://doi.org/10.1016/j.matpr.2018.09.049.
[29] C.R. Cloutier, D.P. Wilkinson, Electrolytic production of hydrogen from aqueous acidic methanol solutions, Int. J. Hydrogen Energy 35 (2010) 3967–3984, https://doi.org/10.1016/j.ijhydene.2010.02.005.
[30] C. Coutanceau, S. Baranton, Electrochemical conversion of alcohols for hydrogen production: a short overview, WIREs Energy Environ 5 (2016) 388–400, https://doi.org/10.1002/wene.193.
[31] Estela Ruiz-López Angel Caravaca, Philippe Vernoux, Fernando Dorado, Antonio de Lucas-Consuegra, over faradaic hydrogen production in a MeOH electrolysis cell, Chem. Eng. J. (2020) 125217. doi: 10.1016/j.cej.2020.125217.
[32] G. Sasikumar, A. Muthumeenal, Sethu Sundar Pethaiah, Nachiappan Nachiappan, Rengarajan Balaji, Aqueous methanol eletrolysis using proton conducting membrane for hydrogen production, Int. J. Hydrogen Energy (2008) 5905–5910, https://doi.org/10.1016/j.ijhydene.2008.07.013.
[33] A.R. de La Osa, A.B. Calcerrada, J.L. Valverde, E.A. Baranova, A. de Lucas-Consuegra, Electrochemical reforming of alcohols on nanostructured platinum-tin catalyst-electrodes, Appl. Catal. B 179 (2015) 276–284, https://doi.org/10.1016/j.apcatb.2015.05.026.
[34] S. Uhm, H. Jeon, Tae Jin Kim, Jaeyoung Lee, Clean hydrogen production from methanol-water solutions via power-saved electrolytic reforming process, J. Power Sources (2012) 218–222, https://doi.org/10.1016/j.jpowsour.2011.09.083.
[35] A. Caravaca, F.M. Sapountzi, A. de Lucas-Consuegra, C. Molina-Mora, F. Dorado, J. L. Valverde, Electrochemical reforming of ethanol-water solutions for pure H_2 production in a PEM electrolysis cell (2012) 9504–9513. doi: 10.1016/j.ijhydene.2012.03.062.
[36] A. Rodríguez-Gómez, F. Dorado, A. de Lucas-Consuegra, Ana Raquel de la Osa, Additional pathways for the ethanol electro-reforming knowledge: the role of the initial concentration on the product yields, Fuel Process. Technol. (2021) 106954, https://doi.org/10.1016/j.fuproc.2021.106954.
[37] A.B. Calcerrada, A.R. de La Osa, J. Llanos, F. Dorado, A. de Lucas-Consuegra, Hydrogen from electrochemical reforming of ethanol assisted by sulfuric acid addition, Appl. Catal. B 231 (2018) 310–316, https://doi.org/10.1016/j.apcatb.2018.03.028.
[38] A.B. Calcerrada, A.R. de La Osa, A. Romero, J.L. Valverde, A. de Lucas-Consuegra, F. Dorado, Optimization of the catalytic support and membrane for the electrochemical reforming of ethanol in alkaline media, J. Chem. Technol. Biotechnol. 94 (2019) 3698–3705, https://doi.org/10.1002/jctb.6175.
[39] Estela Ruiz-López a, Ernesto Amores b, Ana Raquel de la Osa a, Fernando Dorado a, Antonio de Lucas-Consuegra, Electrochemical reforming of ethanol, Chem. Eng. J. (2020) 122289. doi: 10.1016/j.cej.2019.122289.
[40] Ju. HyungKuk, S. Giddey, S.P.S. Badwal, R.J. Mulder, Electro-catalytic conversion of ethanol in solid electrolyte cells for distributed hydrogen generation, Electrochim. Acta (2016) 744–757, https://doi.org/10.1016/j.electacta.2016.07.062.
[41] G. Harzer, PhD Thesis - Gregor Harzer: Boosting High Current Density Performance of Durable, Low Pt-Loaded PEM Fuel Cells, Munich, 2018.
[42] M. Bernt, PhD-Thesis: Analysis of Voltage Losses and Degradation Phenomena in PEM Water Electrolyzers, Munich, 2019.
[43] G.S. Harzer, J.N. Schwämmlein, A.M. Damjanović, S. Ghosh, H.A. Gasteiger, Cathode loading impact on voltage cycling induced PEMFC degradation: a voltage loss analysis, J. Electrochem. Soc. 165 (2018) F3118–F3131, https://doi.org/10.1149/2.0161806jes.
[44] R. Makharia, M.F. Mathias, D.R. Baker, Measurement of catalyst layer electrolyte resistance in PEFCs using electrochemical impedance spectroscopy, J. Electrochem. Soc. 152 (2005) A970, https://doi.org/10.1149/1.1888367.
[45] M. Murbach, B. Gerwe, N. Dawson-Elli, L. Tsui, Impedance.py: A Python package for electrochemical impedance analysis, JOSS 5 (2020) 2349, https://doi.org/10.21105/joss.02349.
[46] M. Pourbaix, Atlas of Electrochemical Equilibria in Aqueous Solutions, National Association Of Corrosion Engineers, 1974.
[47] M.P. Godino, V.M. Barragán, J. Villaluenga, M.A. Izquierdo-Gil, C. Ruiz-Bauzá, B. Seoane, Liquid transport through sulfonated cation-exchange membranes for different water–alcohol solutions, Chem. Eng. J. 162 (2010) 643–648, https://doi.org/10.1016/j.cej.2010.06.013.
[48] F. Waidhas, S. Haschke, P. Khanipour, L. Fromm, A. Görling, J. Bachmann, I. Katsounaros, K.J.J. Mayrhofer, O. Brummel, J. Libuda, Secondary alcohols as rechargeable electrofuels: electrooxidation of isopropyl alcohol at Pt electrodes, ACS Catal. 10 (2020) 6831–6842, https://doi.org/10.1021/acscatal.0c00818.
[49] R. O'Hayre, S.-W. Cha, W. Colella, F.B. Prinz, Fuel Cell Fundamentals, third ed., Wiley, 2016.
[50] E. Teliz, V. Díaz, C.F. Zinola, The enhancement of methanol oxidation electrocatalysis at low and high overpotentials, Electrochim. Acta (2014) 556–565, https://doi.org/10.1016/j.electacta.2014.01.121.
[51] S. Gojković, T.R. Vidaković, D.R. Đurović, Kinetic study of methanol oxidation on carbon-supported PtRu electrocatalyst, Electrochim. Acta 48 (2003) 3607–3614, https://doi.org/10.1016/S0013-4686(03)00481-X.
[52] J.B. Goodenough, l.A. Hamnett, B.J. Kennedy, R. Manoharan, S.A. Weeks, Methanol oxidation on unsupported and carbon supported Pt + Ru anodes, J. Electroanal. Chem. 240 (1988) 133–145, https://doi.org/10.1016/0022-0728(88)80318-8.
[53] Y.-P. Sun, L. Xing, K. Scott, Analysis of the kinetics of methanol oxidation in a porous Pt–Ru anode, J. Power Sources 195 (2010) 1–10, https://doi.org/10.1016/j.jpowsour.2009.07.028.

[54] J. Zhu, F. Cheng, Z. Tao, J. Chen, Electrocatalytic methanol oxidation of Pt 0.5 Ru 0.5-x Sn x /C (x = 0−0.5), J. Phys. Chem. C 112 (2008) 6337–6345. doi: 10.1021/jp8000543.

[55] M. Minichová, C. van Pham, B. Xiao, A. Savan, A. Hutzler, A. Körner, I. Khalakhan, M.G. Rodríguez, I. Mangoufis-Giasin, V. Briega-Martos, A. Kormányos, I. Katsounaros, K.J. Mayrhofer, A. Ludwig, S. Thiele, S. Cherevko, Isopropanol electro-oxidation on Pt-Ru-Ir: A journey from model thin-film libraries towards real electrocatalysts, Electrochim. Acta 444 (2023) 142032, https://doi.org/10.1016/j.electacta.2023.142032.

[56] Iosif Mangoufis-Giasin, Lukáš Fusek, Tian Yang, Peyman Khanipour, Olaf Brummel, Jörg Libuda, Karl J. J. Mayrhofer, Federico Calle-Vallejo, and Ioannis Katsounaros, Activity trends for the selective oxidation of 2-propanol to acetone on noble metal electrodes in alkaline electrolyte, ACS Catal. 13 (2023) 14562–14569. doi: 10.1021/acscatal.3c03423.